

Project report for SCEC Award 21032: “Roles of foreshocks in triggering large earthquakes and stress drop validation”

Xiaowei Chen

Department of Geology and Geophysics, Texas A&M University.

Abstract:

Improved earthquake location and stress drop estimation methods provide great details of the stress drop spatial and temporal variations. Using an improved stacking-based spectral estimation method, we analyzed the stress drop variations for the 2012 Brawley and the 2019 M7 Ridgecrest earthquake sequences. We account for depth-dependent attenuation variations by solving for empirical correction spectrum for events of different depth. For the 2012 Brawley sequence, we find strong geometrical control of stress drop distributions and temporal variations after M5 earthquakes. For the 2019 Ridgecrest sequence, we thoroughly compared the corner frequency and stress drop estimations using different choices of window length and frequency bandwidth, and found variable influences of the result. The choice of window length and wave type also influence the seismic moment estimations, which resulted in different scaling trends.

Intellectual merit:

The research contributes to a better understanding of earthquake source processes and the preparation process for large earthquakes. We find different trends of “foreshock” stress drops for the M7.1 Ridgecrest earthquake and the M5 Brawley earthquakes. The low “foreshock” stress drop for Ridgecrest is consistently found using different wave types and different attenuation corrections. The consistency between the Ridgecrest foreshock and the three other M7 earthquakes in Chen & Shearer (2013) suggests a possible common precursory behavior for large earthquakes. However, the Brawley swarm exhibits more complicated temporal and spatial behaviors before and after M5 earthquakes, suggesting an influence of both internal and external processes. These new results have motivated collaboration between PI and Dr. Jiang to integrate modeling, geodetic observations and seismology to better understand earthquake swarms. The results for the Ridgecrest sequence contributed to the stress drop validation project, contributing to a better understanding of biases and uncertainties of earthquake source parameter estimations.

Broader impacts:

The project results are beneficial for learning earthquake hazards, risks and earthquake physics. The project enabled PI to continue collaborating with former postdoc scholar Qimin Wu, contributed to the training and education of students at the University of Oklahoma, and initiated new collaboration with an earthquake modeler. This project also supported PI Chen’s participation in the Stress drop validation project on the Ridgecrest sequence.

Technical report:

1. Project objective:

We investigate the source processes of two different sequences to understand the roles of “foreshocks”. The 2019 Ridgecrest represents a major tectonic earthquake, while the 2012 Brawley sequence is driven by a shallow aseismic slip due to geothermal operations. Comparison of the two sequences with different dominant triggering processes provides insights into the nucleation and preparation processes of large earthquakes. In addition, we will compare stress drop estimations using different methods (stacking and spectral ratio) and different parameter choices to investigate the influence on stress drop values.

2. Research progress

Data and catalog

For the 2012 Brawley sequence, we download the waveform from SCEDC and update locations using the QTM catalog (Ross et al., 2019). For the 2019 Ridgecrest sequence, we use the dataset provided by the SCEC stress drop validation project.

Stacking analysis:

For each earthquake, we extract P and S waves using 1.5 second and 3 second windows, and calculate the displacement spectrum using multi-taper method. We calculate S-wave spectrum using the geometrical mean of the two horizontal components. Only S-wave spectra with signal-to-noise ratio greater than 2 between 1 and 30 Hz are used for spectral decomposition to obtain event spectra (Shearer et al., 2006). We calibrate low-frequency amplitudes to obtain seismic moments following Shearer et al., (2006). We then apply the improved spectral estimation method from Chen & Abercrombie, (2020) to obtain an empirical correction spectrum, which is used to obtain the attenuation corrected spectrum for each event. For the Ridgecrest sequence, we additionally applied depth-dependent attenuation corrections to mitigate the influence of depth-dependent attenuation variations. We obtain corner frequency estimations using a Brune source model, and use local 1D velocity models to obtain stress drop estimations.

Shearer et al., (2022) focused on relative variations of stress drop in southern California by obtaining the correction spectrum from fitting a fixed stress drop to the lowest magnitude bin for different regions. Slightly differs from their study, we first use the “SNSS” approach in Chen & Abercrombie (2020) to the entire Ridgecrest dataset using stacked spectra for magnitude bins of 0.2 increment. The stress drop value that can simultaneously fit stacked spectra of all magnitude bins is 3.4 MPa, however, the value that produces the lowest standard deviation for all bins is approximately 10 MPa. This indicates a tradeoff between spectral shape and scaling relationship. We use the 10 MPa value that produces the lowest scatter among different magnitude bins, and use this as a fixed value to obtain a correction spectrum for each event using events within 5 km radius epicentral distance and 0.75 depth difference. We focus on the relative variability within the fault zone.

Stacking analysis:

For the Ridgecrest sequence, we also apply spectral ratio method to compare different options: (1) window length, S-wave 3 seconds, 5 seconds, and 10 seconds; (2) frequency bandwidth for spectral fitting: 0.8-25 Hz and 0.2-25 Hz; (3) influence of seismic moment using the S-wave moment from this project and the P-wave seismic moment from Trugman, (2020). The spectral ratio analysis is applied to each event with $M > 3.5$ as target earthquakes, and select events that are within 1 km epicentral distance and depth, and at least 0.75 magnitude smaller as potential EGF events. We follow the procedure in Pennington et al., (2023) to compute spectral ratio and spectral deviation from the Boatwright model. We require a minimum of 5 stations for each target-EGF pair, and require the variance reduction of spectral fitting to be larger than 70%.

Result and Discussion:

1. The influence of parameter choices.

1.1 Comparison of P-wave and S-wave seismic moment calibration

We compare the S-wave spectral magnitude calibration following Shearer et al., (2006) with the P-wave results in Trugman, (2020). The low-frequency spectral amplitudes are converted to moment magnitude by fitting a linear regression with catalog magnitude and assuming $M_l = M_w$ at M_l of 3. Figure 1 shows that there is a systematic difference between P-wave and S-wave results

and the choice of frequency bandwidth for low-frequency amplitude measurement. The choice of time window (5-sec vs 3-sec) only causes minor difference. Results using 0.8-1.5 Hz agree with catalog magnitudes better for larger events, which is expected from the scaling relationship. A strong inconsistency between M3.5 and M4.5 is found between S-wave and P wave results, whereas the S-wave results tend to be higher than catalog magnitude, while the P-wave results tend to be higher. Shearer et al., (2022) discussed the scaling results using P-wave spectral measurement, and suggested that the calibration is no longer valid for $M > 3.5$ earthquakes due to a change from M_l to M_w at a magnitude of 3.5. At lower magnitudes, the S-wave results centered around the catalog magnitudes with some scatter, but the P-wave magnitude systematically differs from catalog magnitude. This could be due to the difference in the scaling relationship between M_w and catalog magnitude in Trugman 2020 and this project: Trugman (2020) obtained a slope ~ 0.75 , while Shearer et al., (2022) and this project found a slope of ~ 1 for earthquakes with $M < 3.5$. It is unclear what causes the systematic differences between different studies using similar methods.

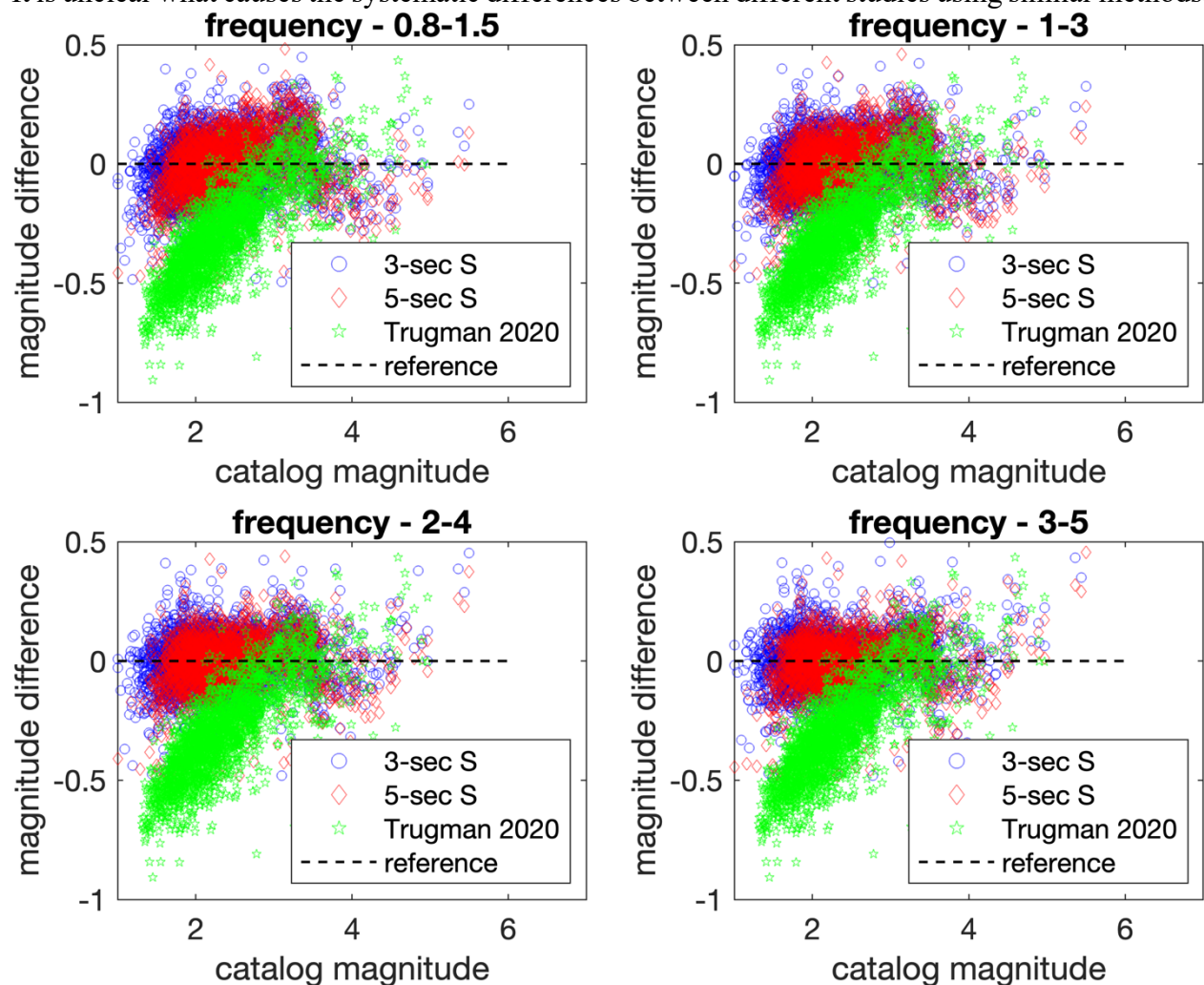


Figure 1. Overview of comparison between calibrated moment magnitude and catalog magnitude (M_l for $M < 3.5$ and M_w for $M > 3.5$ from SCEC) using different choices of time window and frequency bandwidth for low-frequency amplitude measurement. The Y-axis is catalog magnitude – calibrated moment magnitude. Negative means calibrated magnitude is higher than catalog.

1.2 Comparison of scaling trend with seismic moment and depth.

The difference in the S-wave (this project) and P-wave (Trugman, 2020) seismic moment measurements lead to different apparent scaling relationship. Figure 2 shows that the S-wave moment produces no clear scaling relationship for $M < 3.5$ ($M_0 \sim 14$) earthquakes, while the P-wave moment produces a clear continuous scaling relationship for smaller events. Both P and S wave results found strong scaling for larger earthquakes, which could either due to a true physical cause, or the biases in seismic moment calibration for larger events discussed in Shearer et al., (2022). Interestingly, the “narrow-depth-EGF” (using earthquakes within 0.75 km depth range to solve for EGF) also weakens the moment dependence.

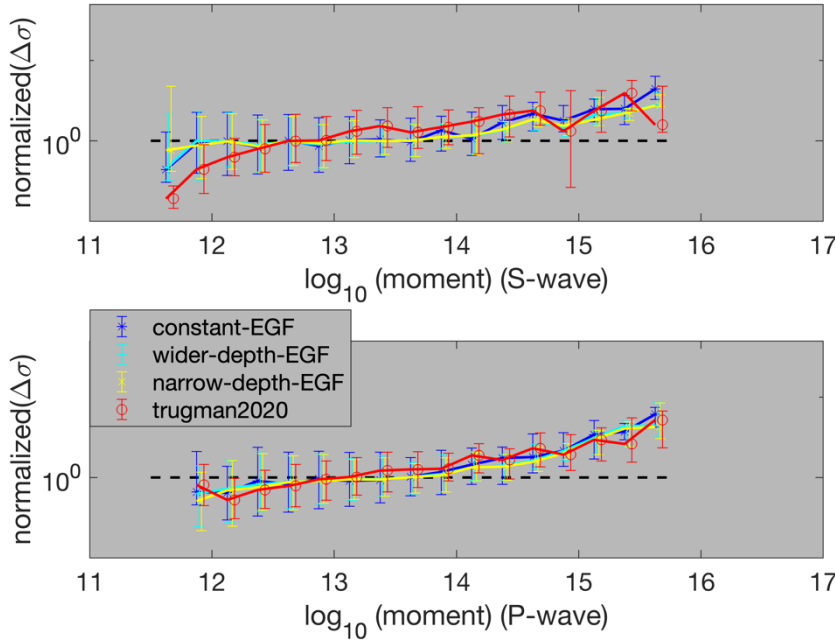


Figure 2. Median stress drop for each magnitude bin of 0.2 with \log_{10} seismic moment. Top uses the S-wave measurement from the 3-sec window and 1-3 Hz. Bottom uses the P-wave moment from Trugman (2020). The “constant-EGF” refers to a single EGF for the entire Ridgecrest area. “wider-depth-EGF” uses depth within 2 km to calculate depth-dependent EGF, while “narrow-depth-EGF” uses 0.75 km as threshold. These two have minor differences, and “narrow-depth-EGF” in the top figure further reduced the scaling behavior at the lower seismic moment.

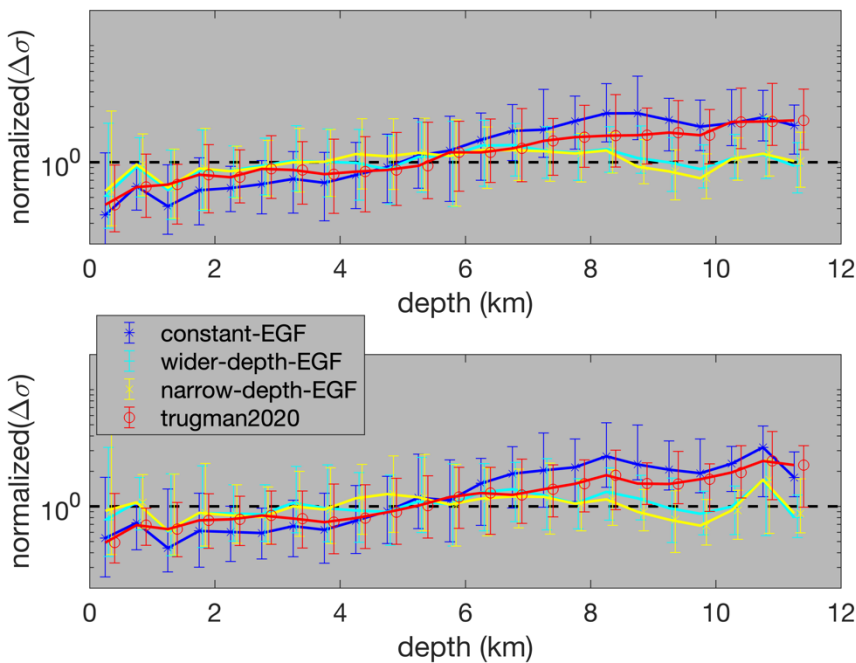


Figure 3. Median stress drop for each depth bin of 0.5 km. Top uses the S-wave measurement from the 3-sec window and 1-3 Hz. Bottom uses the P-wave moment from Trugman (2020). The “constant-EGF” refers to a single EGF for the entire Ridgecrest area. “wider-depth-EGF” uses depth within 2 km to calculate depth-dependent EGF, while “narrow-depth-EGF” uses 0.75 km as threshold. These two have minor differences, and both significantly reduced depth dependence.

The depth dependence is much weaker when applying depth-dependent attenuation correction, which is consistent with Zhang et al., (2022) and Abercrombie et al., (2021).

2. The foreshocks for Ridgecrest and the Brawley earthquake.

Figure 4 shows the stress drop comparison for the “immediate” foreshocks of the M7 earthquake and aftershocks within 1 km epicentral distance of the mainshock. To ensure that the stress drop comparison is not due to depth differences, we also compare the stress drop values of foreshocks to the overall trend of the stress drop variations. We find that the foreshock stress drops are systematically lower than the aftershocks, a similar behavior with the other three M7 earthquakes in Chen & Shearer, (2013). Notably, these foreshock stress drops are lower than the 25% percentile of all earthquakes of the same depth range, suggesting that the relative variability should be robust. Two studies have applied spectral ratio methods to foreshocks of the Hector Mines (Yoon et al., (2019) and the El Mayor Cucapah (Yao et al., 2020) earthquakes, however, they did not compare the stress drop values with aftershocks or the long-term trend. We compared our new foreshock stress drop using the improved stacking method and station coverage for the M7 El Mayor earthquake, and found strong agreement with the spectral ratio results in Yao et al., (2020), suggesting that the foreshock stress drops are reliably measured using the stacking approach. The consistency of the four M7 earthquakes in southern California suggests a possible physical cause of the low stress drop, rather than random fluctuations, and would warrant further assessment, especially comparison with other foreshocks in different tectonic regions.

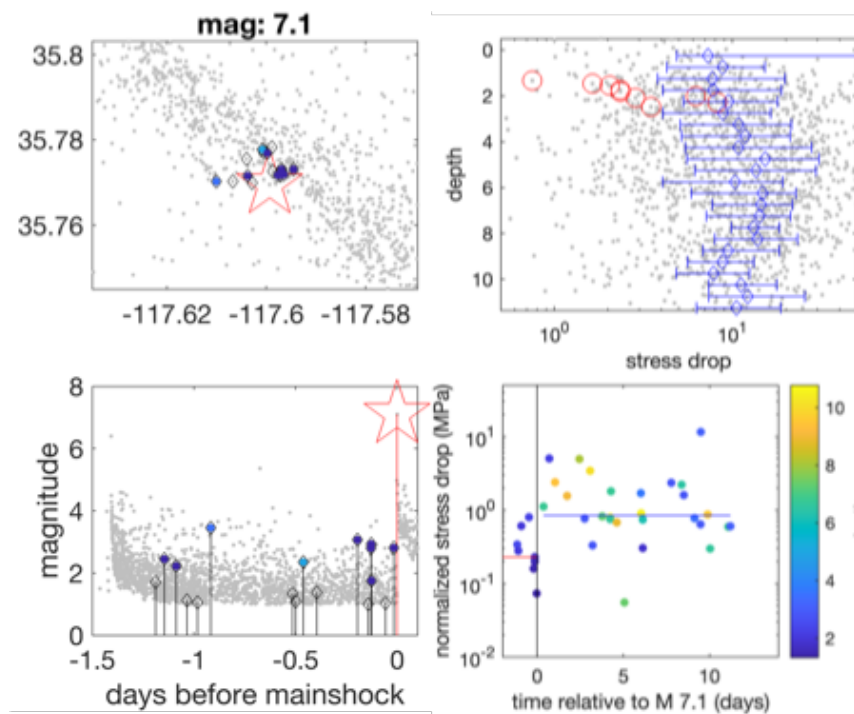


Figure 4. Foreshock stress drop for the M7 Ridgecrest earthquake. Left Column: map view and time view of foreshocks of the M7 mainshock. Open diamonds show all foreshocks within 1 km epicentral distance. Filled diamonds are based on stress drop values. Right Top: Stress drop as a function of depth. The blue diamond and bars show the median, and 25th and 75th percentile of each depth bin. The red circles show the foreshocks. Right Bottom: Stress drop versus time relative to the mainshock. Red and blue lines show the

median stress drop values for foreshock and aftershocks, respectively.

We hypothesize that the foreshocks of the M7 Ridgecrest earthquake are spontaneously triggered within the fault zone due to frictional heterogeneities, similar to the numerical modeling observations (Cattania & Segall, 2021; Ito & Kaneko, 2023). The low stress drop could reflect larger rupture area due to stressing of the creeping patches, which facilitated seismic rupture propagation (Ito & Kaneko, 2023)

This behavior differs from the external aseismic slip driven Brawley swarm in 2012. Using improved stress drop measurement and location, we find that the foreshocks of the M5 earthquakes are located within a high stress drop “asperity” near a geometric complexity, whereas both M5 earthquakes nucleate within the “asperity” (Figure 5). A possible explanation is that the external aseismic slip increased stress loading in the “asperity” due to strength heterogeneity, which caused more energetic foreshocks that lead to the triggering of the mainshock.

Comparison of the two foreshocks driven by different nucleation processes provides insights on how the intrinsic and external factors influence earthquake source processes.

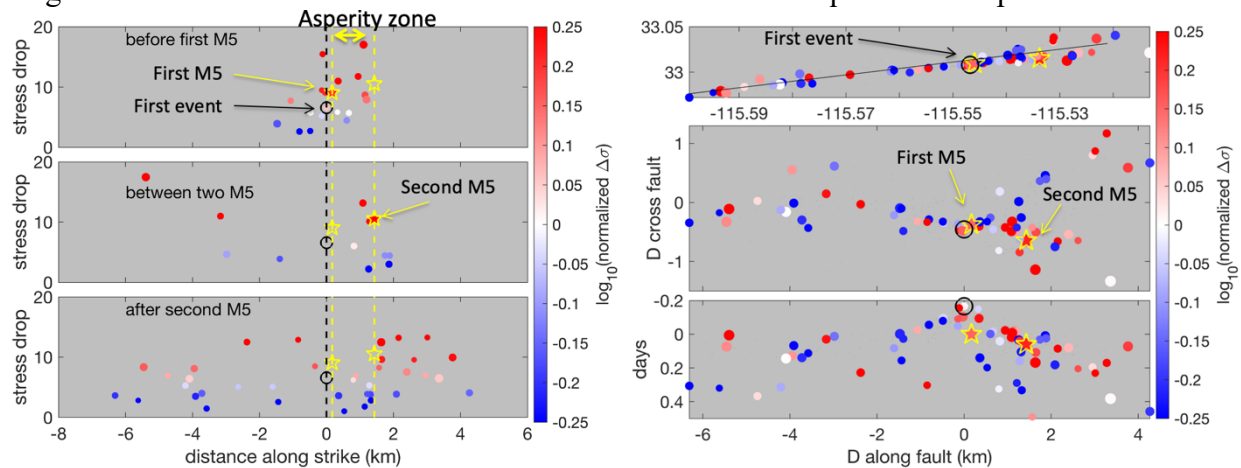


Figure 5. Overview of stress drop in space and time during the 2012 Brawley sequence. Left Column: stress drop VS distance along strike (the black line in Right Top figure) for three time periods: before first M5; between the two M5 earthquakes; after the second M5. The “asperity zone” refers to the area between the two M5 along strike. Right Top: Map view of stress drop distributions. Right Middle: rotated view along strike, which shows that the foreshocks (black circle) denote a slight change in the fault geometry. Right Bottom: Time VS distance along strike to show the migration of foreshocks, and distribution of stress drop.

3. Comparison between stacking and spectral ratio method

Figure 6 shows the comparison of spectral ratio methods using different options with stacking results. We also investigated the influence of source complexity based on results from SCEC project 21169. We find that for $M > 3.5$ earthquakes, simple earthquakes are more consistent among different methods than complex earthquakes, and shorter windows tend to produce smaller scatter than longer windows. Different processing choices of spectral ratio influences the results, and more study is ongoing. Selected events are included in detailed comparison with Dr. Abercrombie and Dr. Huang.

Publication and dissemination:

The Ridgecrest results have been presented at various SCEC stress drop validation workshops and SSA and AGU presentations, and the Brawley results were included in AGU and SSA presentations. Currently working on submission to the BSSA special issue on stress drop validation.

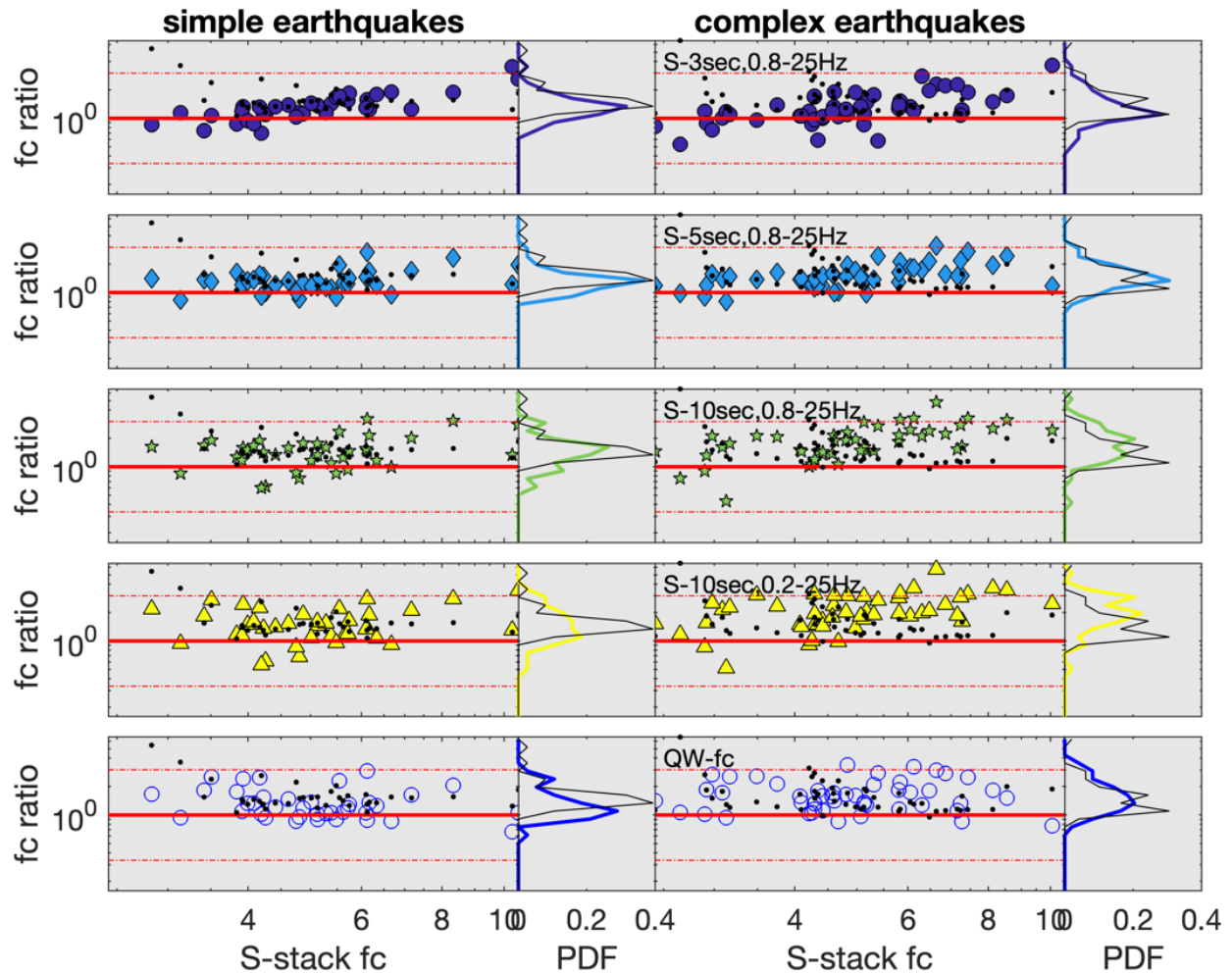


Figure 6. Comparison of different results for simple (left) and complex (right) earthquakes. *QW-fc* refers to the stress drop measurement from SCEC project 21169. For each figure, the red solid line denote 1-1 relationship, and the two thinner lines denote a factor of 1/3 and 3 difference. The Y-axis is the ratio between S-stack *fc* and other *fc* measurements. The black small dots and black lines denote the ratio between S-stack *fc* and P-stack *fc* from Trugman, 2020, and the histogram. Different processing choices are denoted in the text on the right column. The methods in *QW-fc* is described in detail in the report for SCEC 21169, and (Wu et al., 2018).

Reference:

- Cattania, C., & Segall, P. (2021). Precursory Slow Slip and Foreshocks on Rough Faults. *Journal of Geophysical Research: Solid Earth*, 126(4). <https://doi.org/10.1029/2020JB020430>
- Chen, X., & Abercrombie, R. E. (2020). Improved approach for stress drop estimation and its application to an induced earthquake sequence in Oklahoma. *Geophys. J. Int.*, 223, 233–253. <https://doi.org/10.1093/gji/ggaa316>
- Chen, X., & Shearer, P. (2013). California foreshock sequences suggest aseismic triggering process. *Geophys. Res. Lett.*, 40, 2602–2607. <https://doi.org/10.1002/grl.50444>
- Ito, R., & Kaneko, Y. (2023). Physical Mechanism for a Temporal Decrease of the Gutenberg-Richter b-Value Prior to a Large Earthquake. *Journal of Geophysical Research: Solid Earth*, 128(12). <https://doi.org/10.1029/2023JB027413>

- Pennington, C. N., Wu, Q., Chen, X., & Abercrombie, R. E. (2023). Quantifying rupture characteristics of microearthquakes in the Parkfield Area using a high-resolution borehole network. *Geophysical Journal International*, 233(3), 1772–1785. <https://doi.org/10.1093/gji/ggad023>
- Ross, Z. E., Trugman, D. T., Hauksson, E., & Shearer, P. M. (2019). Searching for hidden earthquakes in Southern California. *Science*, 771(May), 767–771. <https://doi.org/10.1126/science.aaw6888>
- Shearer, P. M., Abercrombie, R. E., & Trugman, D. T. (2022). Improved Stress Drop Estimates for M 1.5 to 4 Earthquakes in Southern California From 1996 to 2019. *Journal of Geophysical Research: Solid Earth*, 127(7). <https://doi.org/10.1029/2022JB024243>
- Shearer, P. M., Prieto, G. A., & Hauksson, E. (2006). Comprehensive analysis of earthquake spectral in southern California. *Journal of Geophysical Research-Solid Earth*, 111(B6). <https://doi.org/B0630310.1029/2005jb003979>
- Trugman, D. T. (2020). Stress-drop and source scaling of the 2019 ridgecrest, California, earthquake sequence. *Bulletin of the Seismological Society of America*, 110(4), 1859–1871. <https://doi.org/10.1785/0120200009>
- Wu, Q., Chapman, M. C., & Chen, X. (2018). Stress Drop Variations of Induced Earthquakes in Oklahoma. *Bulletin of the Seismological Society of America*, 108(3A), 1107–1123. <https://doi.org/10.1785/0120170335>
- Yao, D., Huang, Y., Peng, Z., & Castro, R. R. (2020). Detailed Investigation of the Foreshock Sequence of the 2010 Mw7.2 El Mayor-Cucapah Earthquake. *Journal of Geophysical Research: Solid Earth*, 125(6). <https://doi.org/10.1029/2019JB019076>
- Yoon, C. E., Yoshimitsu, N., Ellsworth, W. L., & Beroza, G. C. (2019). Foreshocks and Mainshock Nucleation of the 1999 M w 7.1 Hector Mine, California, Earthquake. *Journal of Geophysical Research: Solid Earth*, 124(2), 1569–1582. <https://doi.org/10.1029/2018JB016383>